

Article

A Comparison of Two Approaches for Estimating the Wheat Nitrogen Nutrition Index Using Remote Sensing

Pengfei Chen ^{1,2}

- ¹ State Key Laboratory of Resources and Environment Information System, Institute of Geographical Science and Natural Resources Research, Chinese Academy of Sciences, Datun Road A11, Chaoyang District, Beijing 100101, China; E-Mail: pengfeichen@igsnr.ac.cn; Tel.: +86-10-6488-9895; Fax: +86-10-6488-9266
- ² Jiangsu Center for Collaborative Innovation in Geographical Information Resource Development and Application, Nanjing 210023, China

Academic Editors: Anton Vrieling and Prasad S. Thenkabail

Received: 14 November 2014 / Accepted: 8 April 2015 / Published: 15 April 2015

Abstract: Remote predictions of the nitrogen nutrition index (*NNI*) are useful for precise nitrogen (N) management in the field. Several studies have recommended two methods for estimating the *NNI*, which are classified as mechanistic and semi-empirical methods in this study. However, no studies have been conducted to thoroughly analyze and compare these two methods. Using winter wheat as an example, this study compared the performances of these two methods for estimating the *NNI* to determine which method is more suitable for practical use. Field measurements were conducted to determine the above ground biomass, N concentration and canopy spectra during different wheat growth stages in 2012. Nearly 120 samples of data were collected and divided into different calibration and validation datasets (containing data from single or multi-growth stages). Based on the above datasets, the performances of the two *NNI* estimation methods were compared, and the influences of phenology on the methods were analyzed. All models that used the mechanistic method with different calibration datasets performed well when validated by validation datasets containing single growth or multi-growth stage data. The validation results had R^2 values between 0.82 and 0.94, root mean square error (*RMSE*) values between 0.05 and 0.17, and *RMSE%* values between 5.10% and 14.41%. Phenology had no effect on this type of *NNI* estimation method. However, the semi-empirical method was influenced by phenology. The performances of the models established using this method were determined by the type of data used for calibration. Thus, the mechanistic method is recommended as a better method

for estimating the *NNI*. By combining proper N management strategies, it can be used for precise N management.

Keywords: *NNI*; remote sensing; nitrogen nutrition diagnosis; winter wheat

1. Introduction

Nitrogen (N) is an essential element for growth and yield of agronomic crops [1]. Because field-supplied N depends on soil, weather and plant conditions, the amount of required N fertilizer often varies in space and time [2]. To ensure productivity, farmers usually apply more N to fields than needed [3]. Supplying excess N not only reduces the income of farmers but also can result in many environmental problems, such as greenhouse gas (N₂O) emissions [4] and surface and ground water contamination [5]. Thus, it is important to optimize fertilization strategies to improve N fertilizer use efficiency.

To enhance N fertilizer use efficiency, many studies have suggested supplying the minimum amount of N required to meet the requirements of crop growth during early growth stages and applying most of the N fertilizer just before rapid, exponential crop growth using topdressing [6]. During latter applications, the crop itself can be used as an indicator of its potential fertilizer N requirements if an adequate indicative parameter can be used. In many studies, the nitrogen nutrition index (*NNI*) has been shown to be a good N status indicator for this purpose [7–9]. The *NNI* is determined by measuring the plant N concentration (expressed on a dry matter basis) and is compared with the critical N concentration. The critical N concentration is defined as the minimum N concentration that is necessary to achieve maximum growth [10] and decreases exponentially as a function of aboveground dry biomass. This concentration function has been determined for many crops and is referred to as the critical N curve [11–13]. When calculating the *NNI*, the critical N concentration is predicted using the critical N curve and the measured aboveground dry biomass as input variables. *NNI* values greater than 1 indicate that the plants are not limited by N, and values lower than 1 indicate N deficiency [14]. However, traditional destructive sampling methods for determining the *NNI* are time consuming and are not practical for use throughout the vegetative growth period under farm conditions [15]. Thus, Lemaire *et al.* suggested using remote sensing measurements to determine the *NNI* because such measurements are rapid and non-destructive and can be repeated multiple times during plant growth [15].

By analyzing the spectral features of the canopy reflectance spectrum, remote sensing technologies have been shown to be powerful tools for predicting crop parameters, especially through spectral indices [16–18]. However, to date, only a few studies have been conducted to estimate the *NNI* using remote sensing. These studies can be classified into two categories. One approach estimates the *NNI* based on its definition. In this method, the plant N concentration, biomass and critical N curve must be known before estimating the *NNI*. Agronomists have determined the critical N curves for many crops, and N concentrations and biomass can be predicted by remote sensing. To estimate N concentrations by remote sensing, the reflectance and transmittance spectra of dried ground leaves were related to the leaf N concentrations, with N absorption features at 1510 nm, 1730 nm, 1940 nm, 1980 nm, 2060 nm, 2180 nm, 2240 nm, 2300 nm and 2350 nm [19,20]. However, field management cannot be conducted

based on those findings because remote sensors are used to collect data over green vegetation rather than dry vegetation. In green vegetation, N absorption features are obscured by strong water absorption bands that are centered at 1450 nm and 1940 nm [21,22]. Because N correlates with chlorophyll in green leaves [23–25], although this relationship is influenced by variables such as species and phenology, the spectral features of chlorophyll in visible and red-edge bands can be used as indicators of crop N. Many N spectral indices have been proposed using these features [1,26]. To estimate biomass using remote sensing, the spectral band, which is significantly influenced by the leaf area index (LAI), can be used because biomass strongly correlates with the LAI. Many LAI spectral indices can be used to estimate biomass [27]. Thus, Chen *et al.* suggested that N concentrations and biomass should be estimated using N and biomass spectral indices, respectively, and in turn used as inputs for *NNI* calculation in model to predict the *NNI* using remote sensing [22]. Because this method uses spectral indices as inputs in a model with a clear theoretical basis, it can be considered a mechanistic method. Few studies have used this method for estimating the *NNI*. By combining an N concentration index referred to as the Double-peak Canopy Nitrogen Index (*DCNI*) and a biomass index referred to as the Red-edge Triangular Vegetation Index (*RTVI*), Chen *et al.* successfully estimated the corn *NNI* in Canada [28]. Using a chlorophyll concentration index referred to as the Modified Chlorophyll Absorption Ratio Index/Modified Triangular Vegetation Index 2 (*MCARI/MTVI2*) and a LAI index named *MTVI2*, Cilia *et al.* attempted to predict the maize *NNI* in Italy through hyperspectral images. However, the authors calculated the actual crop N uptake in the *NNI* formula as the leaf N concentration instead of the plant N concentration [27]. Except for the *NNI* prediction method described above, existing spectral indices have been used to directly assess the *NNI* using semi-empirical models. This method involves the direct creation of a regression model between the *NNI* and the existing spectral indices. Mistele and Schmidhalter estimated the winter wheat *NNI* in Germany using a spectral index called red edge inflection point (*REIP*) [29]. Using linear regression methods, Liang and Liu estimated the *NNI* of corn in China using three spectral indices, the *REIP* and the ratios of reflectance from the band at 740 nm to that at 780 nm and the band at 780 nm to that at 550 nm [30]. This type of *NNI* estimation method can be considered a semi-empirical method.

Currently, no studies have thoroughly analyzed and compared these two methods. However, it is important to understand how these methods are influenced by external factors and which method performs better for practical applications. Thus, winter wheat was used as an example in this study. Based on ground-measured spectra and the corresponding plant N concentrations, biomass and *NNI* during different growth stages, the goals of this study were to (i) test the performances of the above *NNI* prediction methods; (ii) analyze the effects of phenology on their performance; and (iii) suggest a better prediction method for practical use.

2. Data and Methods

2.1. Study Sites and Experimental Design

During the 2011–2012 wheat growing season, a field experiment was conducted to control nitrogen levels and assess the nitrogen status of winter wheat on a farm in the suburbs of Yucheng City (36°33'36", 116°23'24"), which is located on the northwestern plain of Shandong Province, China.

The following three widely used winter wheat cultivars were planted: JiMai 22, KeNong 199 and AiKang 58. N experiments were conducted using three cultivars and five N treatments in a randomized complete block design with four replicates. The soil (0–20 cm) had a loam texture and a pH of 8.0. The average soil organic matter, NO₃-N, available P, and available K contents were 3.1%, 26.3 mg·kg⁻¹, 22.8 mg·kg⁻¹, and 126.0 mg·kg⁻¹, respectively, in the 0–20 cm soil layer before N treatment. The five N fertilization treatments included applications of urea at 0, 70, 140, 210, and 280 kg·N·ha⁻¹. These concentrations were selected based on the local soil N status and other N experiments that were previously conducted in the region. Half of the N was applied at sowing, and half was applied by topdressing during Feekes growth stage 5.0 [31] (3 April 2012). Winter wheat was sown at a density of 4,500,000 plants·ha⁻¹ with a row spacing of 20 cm on 13 October 2011 in 5 by 10 m plots. All of the treated plots received 120 kg·ha⁻¹ P₂O₅ and 80 kg·ha⁻¹ K₂O before sowing and were irrigated during the winter wheat life cycle to prevent water stress.

2.2. Data Acquisition

During the winter wheat growing season, ground-sampling campaigns were conducted on a nearly weekly basis for 8 weeks to monitor the shoot biomass and plant N concentrations. In addition, the corresponding canopy spectra, SPAD (an indicator of chlorophyll content), and LAI values were measured at Feekes growth stages 4 and 7–8. For each sampling campaign, a representative area was selected as the sampling location for each plot. Thus, sixty points were selected for each sampling date.

2.2.1. Remote Sensing Data

The canopy spectra of the wheat were acquired using an Analytical Spectral Devices (ASD) spectroradiometer (Analytical Spectral Devices Inc., Boulder, CO, USA), which recorded the reflectance between 325 nm and 1075 nm over a sampling interval of 1.6 nm with a resolution of 3.5 nm. These measurements were obtained during cloud-free periods between 10 a.m. and 2 p.m. to minimize changes in illumination. A white Spectralon reference panel (Labsphere, North Sutton, NH, USA) was used under the same illumination conditions to convert the spectral radiance measurements to reflectance. Measurements were made at the sampling location in each plot by looking straight down from 1.8 m above the canopy. With a field of view of 25°, the sensor viewed an area with a diameter of 0.8 m, which covered four rows of wheat. Ten scans were measured at each point and averaged to produce the final canopy spectra.

2.2.2. Crop Biophysical and Biochemical Variables

The following biophysical and biochemical variables of the crops were measured at the corresponding spectral sampling points: (1) leaf area index (LAI) using a Sunscan (Delta-T Devies Ltd., Cambridge, England); (2) plant N concentration and biomass using procedures described below; and (3) chlorophyll using a handheld chlorophyll meter (SPAD-502, Minola Osaka Company, Ltd., Osaka, Japan).

To measure the plant N concentrations and biomass, an area of 0.4 × 0.8 m² was harvested in each plot using pruning scissors. Next, the shoot biomass was weighed to obtain the fresh biomass, and a subsample was collected to determine the dry matter content and N concentrations. The subsample was

dried at 65 °C in a forced-draft oven to a constant weight. Next, the material was ground and passed through a 1 mm sieve before storing it at room temperature until analysis. The N concentration was measured using the Dumas Combustion Method with a vario MACRO cube analyzer (Elementar, Hanau, Germany).

2.3. Determination of the *NNI*

The critical N concentration of winter wheat was described using Equation (1), which was based on a recent report of the studied region [32]. The *NNI* was calculated using Equation (2) [33]. In Equations (1) and (2), W is the above ground dry biomass in $\text{Mg}\cdot\text{ha}^{-1}$, N_c is the plant critical N concentration expressed as a percentage of the dry matter, and N_{act} is the actual measured plant N concentration expressed as a percent of the dry matter.

$$N_c = 4.34W^{-0.41} \quad (1)$$

$$NNI = \frac{N_{\text{act}}}{N_c} \quad (2)$$

2.4. Data Analysis

At the Feekes 4 and 7–8 growth stages, the destructively sampled data and corresponding canopy spectra were measured in each replication of the treatments. By considering three cultivars, five N treatments, four replications and two growth stages, 120 paired data points were obtained. This dataset was used for the following analyses.

First, because chlorophyll and the LAI dominate spectral features in the visible and near infrared bands, the relationships between the SPAD values, LAI, plant N concentration, biomass and *NNI* were investigated to determine the principal spectral features of the variables that affected N concentration, biomass and *NNI* predictions using data from each growth stage and all 120 paired data points. Second, for each N treatment on each sampling date, one replication was randomly selected for use as validation data. Thus, 30 paired data points were divided into the validation databases, and the remaining 90 paired data points were considered the calibration database. Third, based on calibration data, the *NNI* estimation models were established using the two *NNI* assessment methods described above. To estimate the *NNI* by the mechanistic method, the N concentration estimation model and biomass estimation model must be established using remote sensing. The following steps were used. (1) Spectral indices considered as good candidates for estimating the plant N concentration and biomass were selected (Table 1 [1,22,34–44] and Table 2 [17,45–52], respectively); (2) To investigate phenology effects, three calibration datasets were produced based on the calibration database that contained data from Feekes 4 and 7–8 growth stages and the two growth stages, respectively. All datasets were used to select the best N concentration estimation index and biomass estimation index; (3) Regarding the N concentration and biomass, three estimation models were constructed using the best index and the three calibration datasets. Using a semi-empirical method to estimate the *NNI*, the following steps were used: (1) the above mentioned three datasets were produced; (2) the relationships between the selected spectral indices and *NNI* were examined using the three datasets, respectively, and the best index for *NNI* assessment was selected; and (3) three *NNI* estimation models were established using the best index and three calibration datasets. Finally, the validation database was used to test the performances of the models established using the

two *NNI* assessment methods. During this process, the validation database was used to produce three validation datasets to investigate the phenology effects. These datasets contain data from Feekes 4 and 7–8 growth stages and both growth stages. Each validation dataset was used to test the performances of the models established using the two *NNI* assessment methods. The determination coefficient (R^2), root mean square error (*RMSE*) and relative *RMSE* ($RMSE/\text{average mean} \times 100$, *RMSE%*) were used to evaluate the model performances throughout the procedure.

3. Results and Analyses

3.1. Relationships between the SPAD, LAI, Plant N Concentration and *NNI* Values

Because water absorption obscures N absorption features in the shortwave bands, it is difficult to detect plant N concentrations from N absorption features in this portion of the electromagnetic spectrum [22]. Thus, it is appropriate to use reflectance in the visible and red-edge bands to estimate N concentrations based on the good relationships between chlorophyll concentrations and plant N concentrations. In addition, biomass has a good relationship with the LAI in green vegetation, and the *NNI* is calculated using the N concentration, biomass and a known critical N curve. The relationships among the SPAD, LAI, plant N concentration, biomass and *NNI* values were assessed because the visible and near infrared reflectance are dominated by the LAI and chlorophyll absorption features.

Significant correlations ($p < 0.01$) were found between the SPAD values and plant N concentrations in the three datasets (Table 3 and Figure 1a). Cartelat *et al.* and Chen *et al.* also observed a significant correlation between the chlorophyll and N concentrations in wheat [22,25]. In this study, the LAI had a weak relationship with plant N concentration in the dataset containing data from all growth stages, although the relationship was significant. In addition, the LAI was strongly related to the plant N concentration in the dataset that contained data from the single growth stage. As the crop grows, from planting to biophysical maturity, crop N and chlorophyll concentration decrease as the biomass and LAI increase [13]. For a given growth stage, the plant N concentration and LAI change consistently, according to the variation in the available N in the field. Thus, on the one hand, the plant N concentration is strongly related to both the LAI and chlorophyll in the dataset that contained data from a single growth stage. On the other hand, the plant N concentration was weakly related to the LAI in the dataset that contained data from multiple growth stages. Thus, the following conclusions can be obtained that: (1) the spectral feature of chlorophyll can be used to estimate the N concentration and (2) the LAI influence is a confounding factor for remotely assessing the N concentration at different growth stages.

Table 1. Summary of the studied spectral indices for predicting plant nitrogen (N) concentration.

Index	Name	Formula	Developed by
<i>Nitrogen Indices</i>			
$V_{i_{opt}}$	Optimal Vegetation Index	$(1 + 0.45)((R_{800})^2 + 1)/(R_{670} + 0.45)$	Reyniers <i>et al.</i> [34]
$RVI I^\dagger$	Ratio Vegetation Index I	R_{810}/R_{660}	Zhu <i>et al.</i> [1]
$RVI II^\dagger$	Ratio Vegetation Index II	R_{810}/R_{560}	Xue <i>et al.</i> [35]
<i>MCARI/MTVI2</i>			
<i>MCARI/MTVI2</i>	Combined Index	$MCARI: (R_{700} - R_{670} - 0.2(R_{700} - R_{550}))(R_{700}/R_{670})$ $MTVI2: 1.5(1.2(R_{800} - R_{550}) - 2.5(R_{670} - R_{550}))/$ $\text{sqrt}((2R_{800} + 1)^2 - (6R_{800} - 5\text{sqrt}(R_{670})) - 0.5)$	Eitel <i>et al.</i> [36]
<i>REIP-LE</i>	Red Edge Inflection Point: Linear Extrapolation Method	Based on the linear extrapolation of two straight lines through two points on the far-red and two points on the NIR flanks of the first derivative reflectance spectrum of the red edge region. The REIP is defined by the wavelength value at the intersection of the straight lines.	Cho and Skidmore [37]
<i>DCNI</i>	Double-Peak Canopy Nitrogen Index	$(R_{720} - R_{700})/(R_{700} - R_{670})/(R_{720} - R_{670} + 0.03)$	Chen <i>et al.</i> [22]
<i>Chlorophyll Indices</i>			
<i>MCARI</i>	Modified Chlorophyll Absorption Ratio Index	$(R_{700} - R_{670} - 0.2(R_{700} - R_{550}))(R_{700}/R_{670})$	Daughtry <i>et al.</i> [38]
<i>TCARI</i>	Transformed Chlorophyll Absorption in Reflectance Index	$3((R_{700} - R_{670}) - 0.2(R_{700} - R_{550}))(R_{700}/R_{670})$	Haboudane <i>et al.</i> [39]
<i>TCARI/OSAVI</i>			
<i>TCARI/OSAVI</i>	Combined Index II †	$TCARI: 3((R_{700} - R_{670}) - 0.2(R_{700} - R_{550}))(R_{700}/R_{670})$ $OSAVI: 1.16(R_{800} - R_{670})/(R_{800} + R_{670} + 0.16)$	Haboudane <i>et al.</i> [40]
<i>MTCI</i>	MERIS Terrestrial Chlorophyll Index	$(R_{750} - R_{710})/(R_{710} - R_{680})$	Dash and Curran [41]
$R-M^\dagger$	Red Model	$R_{750}/R_{720} - 1$	Gitelson <i>et al.</i> [42]
<i>CCI</i>	Canopy Chlorophyll Index	D_{720}/D_{700}	Sims <i>et al.</i> [43]
<i>REIP-LI</i>	Red Edge Inflection Point: Linear Interpolation Method	$700 + 40(R_{re} - R_{700})/(R_{740} - R_{700})$ $R_{re}: (R_{670} + R_{780})/2$	Guyot <i>et al.</i> [44]

R_i indicates the reflectance at band i (nanometer); † indicates named by Chen *et al.* [22]; D_i indicates derivative reflectance at band i (nanometer).

Table 2. Summary of the studied spectral indices for predicting above ground biomass.

Index	Name	Formula	Developed by
<i>LAI Indices</i>			
<i>NDVI</i>	Normalized Difference Vegetation Index	$(R_{800} - R_{670}) / (R_{800} + R_{670})$	Rouse <i>et al.</i> [45]
<i>RVI</i>	Ratio Vegetation Index	R_{800} / R_{670}	Pearson <i>et al.</i> [46]
<i>EVI</i>	Enhanced Vegetation Index	$2.5(R_{800} - R_{670}) / (R_{800} + 6R_{670} - 7.5R_{470} + 1)$	Huete <i>et al.</i> [47]
<i>TVI</i>	Triangular Vegetation Index	$0.5(120(R_{750} - R_{550}) - 200(R_{670} - R_{550}))$	Broge and Leblanc [48]
<i>MSAVI</i>	Modified Soil-Adjusted Vegetation Index	$(2R_{800} + 1 - \sqrt{(2R_{800} + 1)^2 - 8(R_{800} - R_{670})}) / 2$	Qi <i>et al.</i> [49]
<i>OSAVI</i>	Optimization of Soil-Adjusted Vegetation Index	$1.16(R_{800} - R_{670}) / (R_{800} + R_{670} + 0.16)$	Rondeaux <i>et al.</i> [50]
<i>GNDVI</i>	Green Normalized Difference Vegetation Index	$(R_{800} - R_{550}) / (R_{800} + R_{550})$	Gitelson <i>et al.</i> [51]
<i>MTVI2</i>	Modified Triangular Vegetation Index 2	$1.5(1.2(R_{800} - R_{550}) - 2.5(R_{670} - R_{550})) / \sqrt{(2R_{800} + 1)^2 - (6R_{800} - 5\sqrt{R_{670}}) - 0.5}$	Haboudance <i>et al.</i> [17]
<i>Biomass Indices</i>			
<i>RTVI</i>	Red-Edge Triangular Vegetation Index	$(100(R_{750} - R_{730}) - 10(R_{750} - R_{550}))\sqrt{R_{700}/R_{670}}$	Chen <i>et al.</i> [52]

R_i indicates the reflectance at band i (nanometer).

Table 3. Correlation matrix among the SPAD, leaf area index (LAI), plant N concentration, biomass and nitrogen nutrition index (NNI) values.

Spectral Index	Biomass	LAI	N Concentration	SPAD	NNI
<i>Data from all growth stages (n = 120)</i>					
Biomass	1.00				
LAI	0.93 *	1.00			
N concentration	0.19	0.25 *	1.00		
SPAD	0.05	0.07	0.77 *	1.00	
NNI	0.73 *	0.74 *	0.80 *	0.47 *	1.00
<i>Data from Feekes 4 (n = 60)</i>					
Biomass	1.00				
LAI	0.76 *	1.00			
N concentration	0.64 *	0.73 *	1.00		
SPAD	0.52 *	0.60 *	0.70 *	1.00	
NNI	0.87 *	0.81 *	0.93 *	0.68 *	1.00
<i>Data from Feekes 7–8 (n = 60)</i>					
Biomass	1.00				
LAI	0.84 *	1.00			
N concentration	0.69 *	0.87 *	1.00		
SPAD	0.66 *	0.70 *	0.80 *	1.00	
NNI	0.83 *	0.92 *	0.97 *	0.80 *	1.00

n indicates number of samples; * denotes significance at the 0.01 level.

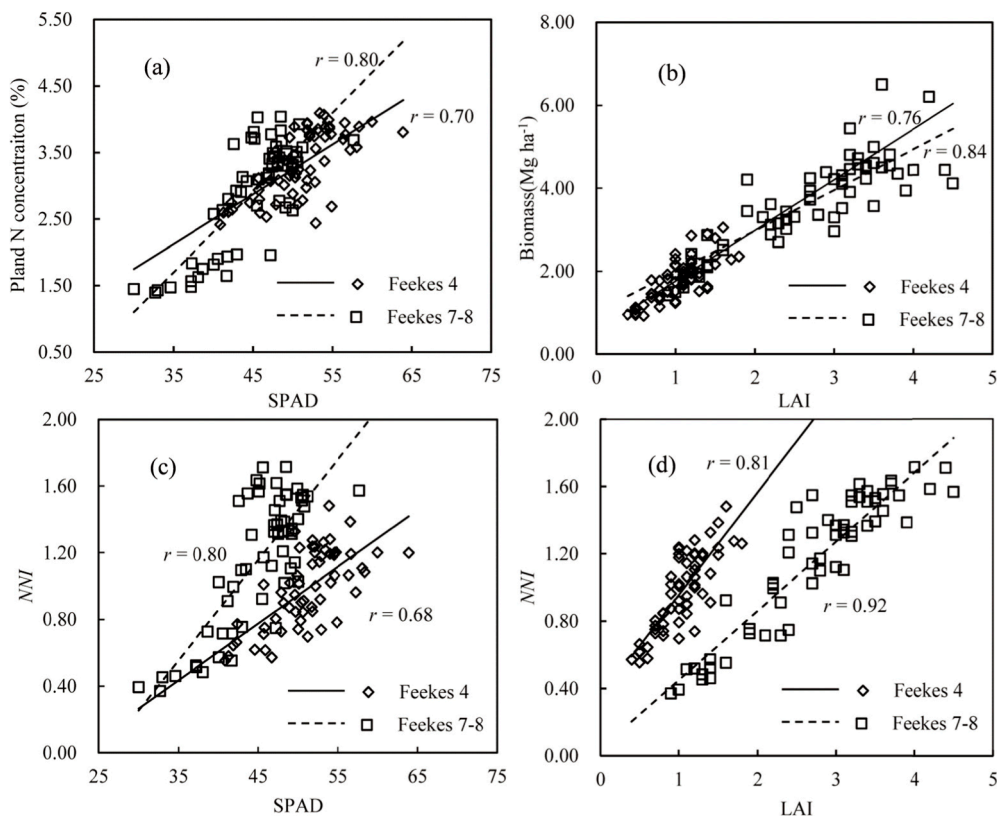


Figure 1. Correlation matrices between (a) plant nitrogen concentration (%) and SPAD values; (b) biomass and LAI; (c) *NNI* and SPAD values; and (d) *NNI* and LAI.

Significant correlations ($p < 0.01$) were observed between the biomass and LAI in the three datasets (Table 3 and Figure 1b). Lemaire *et al.* also found a good relationship between biomass and the LAI [53]. In this study, the SPAD value did not significantly correlate with biomass when using the data from all growth stages. However, a significant relationship was observed with biomass when using the data from a single growth stage. The reason for the relationship between N concentration and the LAI also applies to the relationship between biomass and the SPAD value. As the crop grows, the crop N and chlorophyll concentrations decrease as the biomass and LAI increase [13]. For a given growth stage, biomass and chlorophyll consistently change as the available N in the field varies. Thus, biomass is significantly related to both the LAI and SPAD values in the dataset containing data from a single growth stage. In addition, the biomass showed no significant relationship with the SPAD in the dataset that contained data from multiple growth stages. Therefore, the following conclusions were made: (1) The spectral bands influenced by the LAI can be used for biomass estimation; and (2) the spectral feature of chlorophyll is a confounding factor for remotely assessing biomass at different growth stages.

Significant correlations ($p < 0.01$) were observed between the LAI and *NNI* and between the SPAD values and *NNI* in the three datasets (Table 3). These relationships most likely occurred because the *NNI* is calculated using biomass and N concentration. Although significant correlations were found, they were influenced by phenology (Figure 1c,d). The data points from two growth stages were gathered into two groups. Thus, (1) both spectral features influenced by the LAI and chlorophyll can be used to estimate the *NNI*; and (2) the influences of phenology must be considered when creating a *NNI* prediction model that uses the spectral features influenced by the LAI or chlorophyll.

3.2. The NNI Estimation Model Using a Mechanistic Method

To select the best indices for estimating the plant N concentration, a correlation analysis was performed using three calibration datasets. When a significant correlation ($p < 0.01$) was observed between the indices and the plant N concentrations, linear, exponential, power, and logarithmic models were tested for the regression analysis. The R^2 values, RMSE values, RMSE% values and model types of the best model are reported in Table 4, which indicates that the best relationships occurred when the MCARI/MTVI2 was used. The regression equation for the MCARI/MTVI2 had an R^2 value of 0.62, RMSE value of 0.46, and RMSE% value of 14.74% when using calibration data from all growth stages, an R^2 value of 0.61, RMSE value of 0.33, and RMSE% value of 9.91% when using calibration data from Feekes 4 growth stage, and an R^2 value of 0.72, RMSE value of 0.48, and RMSE% value of 16.55% when using calibration data from Feekes 7–8 growth stage. To obtain a good estimation of the N concentration, the spectral index should be correlated with the N concentration and show low sensitivity to other confounding factors [38]. The LAI had a limited influence on the MCARI/MTVI2, with a weak relationship with LAI using calibration data from different growth stages ($R^2 = 0.26$).

Table 4. Regression analysis between the N-related spectral indices and plant N concentrations. Linear(Lin), logarithmic(Log), exponential(Exp), and power(Pow) models were used for fitting the data. The results [R^2 , RMSE(%) and RMSE%] of the best calibration models are shown.

Spectral Index	N Concentration		LAI	
	R^2 (Model Type)	RMSE (RMSE%)	R^2 (Model Type)	RMSE (RMSE%)
<i>Using data from all growth stages (n = 90)</i>				
$V_{i_{opt}}$	0.13 (Log)	0.67 (21.47%)	0.90 (Pow)	0.47 (25.00%)
RV_{II}	0.09 (Log)	0.68 (21.79%)	0.90 (Pow)	0.53 (28.19%)
$RV_{I\ II}$	0.13 (Pow)	0.68 (21.79%)	0.90 (Pow)	0.50 (26.60%)
MCARI/MTVI2	0.62 (Exp)	0.46 (14.74%)	0.26 (Pow)	0.98 (52.13%)
REIP-LE	0.36 (Pow)	0.60 (19.23%)	0.56 (Pow)	0.75 (39.89%)
DCNI	0.43 (Pow)	0.59 (18.91%)	0.41 (Lin)	0.87 (46.28%)
MCARI	–	–	0.64 (Pow)	0.76 (40.43%)
TCARI	0.12 (Exp)	0.70 (22.44%)	0.15 (Pow)	1.08 (57.45%)
TCARI/OSAVI	0.37 (Exp)	0.60 (19.23%)	0.59 (Pow)	0.76 (40.43%)
MTCI	0.32 (Pow)	0.61 (19.55%)	0.80 (Lin)	0.56 (29.79%)
R-M	0.17 (Log)	0.65 (20.83%)	0.89 (Pow)	0.50 (26.60%)
CCI	0.31 (Log)	0.59 (18.91%)	0.49 (Exp)	0.85 (45.21%)
REIP-LI	0.32 (Pow)	0.63 (20.19%)	0.77 (Exp)	0.55 (29.26%)
<i>Using data from the Feekes 4 growth stage (n = 45)</i>				
$V_{i_{opt}}$	0.55 (Lin)	0.34 (10.21%)	0.77 (Pow)	0.17 (16.19%)
RV_{II}	0.55 (Log)	0.35 (10.51%)	0.76 (Log)	0.16 (15.24%)
$RV_{I\ II}$	0.59 (Log)	0.33 (9.91%)	0.80 (Log)	0.14 (13.23%)
MCARI/MTVI2	0.61 (Log)	0.33 (9.91%)	0.67 (Exp)	0.21 (20.00%)
REIP-LE	0.48 (Lin)	0.37 (11.11%)	0.60 (Pow)	0.24 (22.86%)
DCNI	0.51 (Log)	0.37 (11.11%)	0.42 (Pow)	0.25 (23.81%)
MCARI	0.20 (Pow)	0.47 (14.11%)	0.40 (Pow)	0.26 (24.76%)
TCARI	–	–	0.25 (Pow)	0.29 (27.62%)
TCARI/OSAVI	0.59 (Log)	0.33 (9.91%)	0.67 (Exp)	0.20 (19.05%)
MTCI	0.65 (Log)	0.31 (9.31%)	0.83 (Pow)	0.15 (14.29%)
R-M	0.61 (Log)	0.33 (9.91%)	0.84 (Pow)	0.14 (13.33%)
CCI	0.56 (Lin)	0.35 (10.51%)	0.45 (Pow)	0.25 (23.81%)
REIP-LI	0.65 (Lin)	0.31 (9.31%)	0.81 (Exp)	0.20 (19.05%)

Table 4. Cont.

Spectral Index	N Concentration		LAI	
	R^2 (Model Type)	RMSE (RMSE%)	R^2 (Model Type)	RMSE (RMSE%)
<i>Using data from the Feekes 7–8 growth stage (n = 45)</i>				
$V_{i_{opt}}$	0.86 (Pow)	0.36 (12.41%)	0.84 (Pow)	0.59 (21.61%)
<i>RVI I</i>	0.78 (Pow)	0.45 (15.52%)	0.81 (Pow)	0.68 (24.91%)
<i>RVI II</i>	0.83 (Pow)	0.40 (13.79%)	0.84 (Pow)	0.65 (23.81%)
<i>MCARI/MTVI2</i>	0.72 (Pow)	0.48 (16.55%)	0.75 (Exp)	0.71 (26.01%)
<i>REIP-LE</i>	0.76 (Exp)	0.45 (15.52%)	0.67 (Pow)	0.73 (26.74%)
<i>DCNI</i>	0.65 (Pow)	0.56 (19.31%)	0.71 (Pow)	0.79 (28.94%)
<i>MCARI</i>	–	–	–	–
<i>TCARI</i>	0.23 (Exp)	0.75 (25.86%)	0.31 (Exp)	0.93 (34.07%)
<i>TCARI/OSAVI</i>	0.67 (Pow)	0.54 (18.62%)	0.76 (Exp)	0.74 (27.11%)
<i>MTCI</i>	0.85 (Exp)	0.39 (13.45%)	0.88 (Pow)	0.61 (22.34%)
<i>R-M</i>	0.84 (Pow)	0.38 (13.10%)	0.82 (Pow)	0.63 (23.08%)
<i>CCI</i>	0.63 (Pow)	0.51 (17.59%)	0.53 (Pow)	0.79 (28.94%)
<i>REIP-LI</i>	0.86 (Exp)	0.42 (14.48%)	0.89 (Pow)	0.62 (22.71%)

– indicates that significant ($p < 0.01$) correlations were not observed between the two variables; n indicates the sample number.

The good relationships between the MCARI/MTVI2 and LAI when using calibration data from a single growth stage occurred because the plant N concentration and LAI changed consistently during a given growth stage with variations in available N in the field (Table 3). The second best relationship was observed between the DCNI and the plant N concentration. The regression equations of the DCNI had an R^2 value of 0.43, RMSE value of 0.59, and RMSE% value of 18.91% when using calibration data from all growth stages, an R^2 value of 0.51, RMSE value of 0.37, and RMSE% value of 11.11% when using calibration data from Feekes 4 growth stage, and an R^2 value of 0.65, RMSE value of 0.56, and RMSE% value of 19.31% when using calibration data from Feekes 7–8 growth stage, respectively. The Transformed Chlorophyll Absorption in Reflectance Index (TCARI) and MCARI had little or no relationship with the N concentrations of the three datasets. Other indices had medium or good relationships with the N concentrations, with R^2 values between 0.48 and 0.86, RMSE values between 0.31 and 0.54, and RMSE% values between 9.31% and 18.62% when using calibration data from the single growth stage. Meanwhile, these indices had weak or moderate relationships with the N concentrations with R^2 values between 0.09 and 0.37, RMSE values between 0.59 and 0.68, and RMSE% values between 18.91% and 21.79% when using calibration data from all growth stage. The LAI had a strong influence on these indices, which have good correlative relationships with the LAI. Thus, the MCARI/MTVI2 was selected to estimate the N concentrations when using the mechanistic NNI estimation method, and a scatterplot for the MCARI/MTVI2 vs. N concentration is shown in Figure 2a.

To select the best indices for estimating biomass, the previously described procedure was used and the relationships between the selected biomass-related spectral indices and biomass were analyzed. The results are listed in Table 5, which shows that all of the tested spectral indices had good correlations with biomass in the three calibration datasets. Meanwhile, the correlations between the tested indices and SPAD values were not significant when using calibration data from all growth stages, which indicated that chlorophyll does not significantly influence the performances of these indices for estimating biomass. The good relationships between the tested indices and SPAD values when using calibration

data from a single growth stage occur because the biomass and chlorophyll levels consistently change during a given growth stage with the variation of available N in the field (Table 3). Among all of the indices, the RTVI performed best for assessing biomass, with an R^2 value of 0.85, RMSE value of 0.53, and RMSE% value of 19.27% when using calibration data from all growth stages, an R^2 value of 0.80, RMSE value of 0.24, and RMSE% value of 13.19% when using calibration data from Feekes 4 growth stage, and an R^2 value of 0.73, RMSE value of 0.59, and RMSE% value of 15.99% when using calibration data from Feekes 7–8 growth stage, respectively. The regression equations between biomass and the other indices had R^2 values between 0.79 and 0.86, RMSE values between 0.51 and 0.63, and RMSE% values between 18.55% and 22.91% when using calibration data from all growth stages, R^2 values between 0.75 and 0.80, RMSE values between 0.24 and 0.28, and RMSE% values between 13.19% and 15.38% when using calibration data from the Feekes 4 growth stage, and R^2 values between 0.60 and 0.72, RMSE values between 0.61 and 0.68, and RMSE% values between 16.53% and 18.43% when using calibration data from the Feekes 7–8 growth stage. Additionally, the Normalized Difference Vegetation Index (NDVI), the Enhanced Vegetation Index (EVI), the Modified Soil-Adjusted Vegetation Index (MSAVI) and the Optimization of Soil-Adjusted Vegetation Index (OSAVI) are NDVI-like spectral indices that have been criticized because they can easily become saturated when the biomass content is medium to high [54]. Chen *et al.* reported that the Triangular Vegetation Index (TVI), Green NDVI (GNDVI), and Modified Triangular Vegetation Index 2 (MTVI2) were also easily saturated under medium to high biomass [52]. The biomass data in this study were measured at Feekes 4 and Feekes 7–8 growth stages, and it is important to apply N by topdressing between these two growth stages. The wheat biomass during this period was not high. Thus, the EVI, TVI, MSAVI and MTVI2 did not present saturation issues in this study. However, the NDVI, OSAVI and GNDVI were saturated more easily, and these indices exhibited saturation when using the data in this study with high biomass contents (data not shown). Finally, the RTVI was selected for estimating biomass, and a scatterplot for the RTVI and biomass is shown in Figure 2b.

Table 5. Regression analysis results between the biomass-related spectral indices and biomass. Linear, logarithmic, exponential, and power models were used for fitting. The results (R^2 , $RMSE(Mg \cdot ha^{-1})$ and $RMSE\%$) of the best calibration models are shown.

Spectral Index	Biomass		SPAD	
	R^2 (Model Type)	$RMSE$ ($RMSE\%$)	R^2 (Model Type)	$RMSE$ ($RMSE\%$)
<i>Using data from all growth stages (n = 90)</i>				
NDVI	0.86 (Exp)	0.53 (19.27%)	–	–
RVI	0.85 (Pow)	0.53 (19.27%)	–	–
EVI	0.82 (Pow)	0.58 (21.09%)	–	–
TVI	0.79 (Pow)	0.63 (22.91%)	–	–
MSAVI	0.84 (Pow)	0.55 (20.00%)	–	–
OSAVI	0.86 (Exp)	0.52 (18.91%)	–	–
GNDVI	0.86 (Exp)	0.51 (18.55%)	–	–
MTVI2	0.85 (Pow)	0.54 (19.64%)	–	–
RTVI	0.85 (Pow)	0.53 (19.27%)	–	–

Table 5. Cont.

Spectral Index	Biomass		SPAD	
	R^2 (Model Type)	RMSE (RMSE%)	R^2 (Model Type)	RMSE (RMSE%)
<i>Using data from the Feekes 4 growth stage (n = 45)</i>				
NDVI	0.78 (Pow)	0.25 (13.74%)	0.34 (Pow)	4.30 (8.42%)
RVI	0.75 (Log)	0.25 (13.74%)	0.25 (Pow)	4.22 (8.26%)
EVI	0.78 (Pow)	0.26 (14.29%)	0.32 (Pow)	4.04 (7.91%)
TVI	0.75 (Pow)	0.28 (15.38%)	0.29 (Pow)	4.13 (8.09%)
MSAVI	0.78 (Pow)	0.26 (14.29%)	0.31 (Pow)	4.06 (7.95%)
OSAVI	0.78 (Pow)	0.26 (14.29%)	0.33 (Pow)	4.00 (7.83%)
GNDVI	0.80 (Pow)	0.24 (13.19%)	0.39 (Pow)	3.83 (7.50%)
MTVI2	0.78 (Pow)	0.26 (14.29%)	0.30 (Pow)	4.09 (8.01%)
RTVI	0.80 (Pow)	0.24 (13.19%)	0.40 (Pow)	3.82 (7.48%)
<i>Using data from the Feekes 7–8 growth stage (n = 45)</i>				
NDVI	0.65 (Pow)	0.65 (17.62%)	0.60 (Pow)	3.47 (7.70%)
RVI	0.63 (Pow)	0.64 (17.34%)	0.54 (Pow)	3.75 (8.33%)
EVI	0.66 (Pow)	0.64 (17.34%)	0.61 (Pow)	3.49 (7.75%)
TVI	0.60 (Pow)	0.68 (18.43%)	0.55 (Pow)	3.75 (8.33%)
MSAVI	0.67 (Pow)	0.63 (17.07%)	0.62 (Pow)	3.44 (7.64%)
OSAVI	0.68 (Pow)	0.63 (17.07%)	0.63 (Pow)	3.39 (7.53%)
GNDVI	0.72 (Pow)	0.61 (16.53%)	0.68 (Pow)	3.20 (7.10%)
MTVI2	0.66 (Pow)	0.63 (17.07%)	0.61 (Pow)	3.50 (7.77%)
RTVI	0.73 (Pow)	0.59 (15.99%)	0.66 (Pow)	3.31 (7.35%)

– indicates that significant ($p < 0.01$) correlations were not observed between the two variables; n indicates sample number.

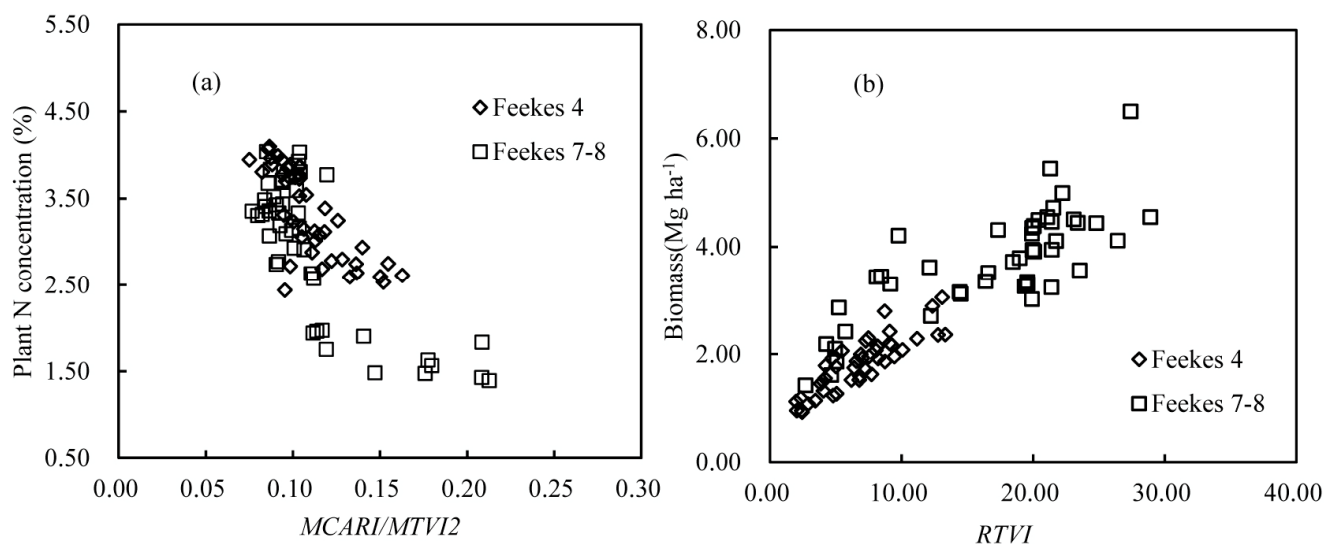


Figure 2. Scatterplots for (a) MCARI/MTVI2 vs. N concentration and (b) RTVI vs. biomass.

Finally, based on the N concentration estimation model of the *MCARI/MTVI2* and the biomass estimation model of the *RTVI*, the *NNI* values were assessed using the three calibration datasets. The relationship between the estimated and actual *NNI* had an R^2 value of 0.83, *RMSE* value of 0.10 and *RMSE%* value of 10.37% when using calibration data from Feekes 4 growth stage, an R^2 value of 0.78, *RMSE* value of 0.19 and *RMSE%* value of 16.09% when using calibration data from the Feekes 7–8

growth stage, and an R^2 value of 0.83, $RMSE$ value of 0.14 and $RMSE\%$ value of 13.24% when using calibration data from all growth stages. In Figure 3, points are noted that represent the estimated and actual NNI values that were assessed using the three different calibration models. These points were clustered together, which indicated no phenology influences on the mechanistic NNI estimation method.

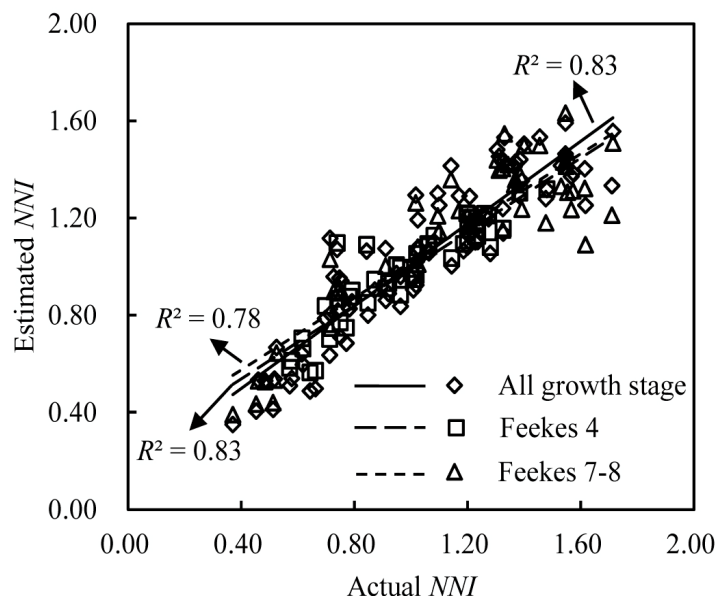


Figure 3. Calibration results of the mechanistic NNI estimation method when using three calibration datasets.

3.3. The NNI Estimation Model Using a Semi-Empirical Method

To select the best index for estimating the NNI using the semi-empirical method, a correlation analysis was performed using the three calibration datasets. When a significant correlation ($p < 0.01$) occurred between the indices and NNI , linear, exponential, power, and logarithmic regression models were tested. The R^2 values, $RMSE$ values, $RMSE\%$ values and model types of the best model are reported in Table 6. Except for the $MCARI$ and $TCARI$, all of the selected indices resulted in medium to high correlations with the NNI . These relationships occurred because of the good relationships between the NNI and chlorophyll, and between the NNI and LAI (Table 3). Among these indices, the $REIP-LI$ and $MTCI$ exhibited the best results. The regression equation between the $REIP-LI$ and NNI had an R^2 value of 0.80, an $RMSE$ value of 0.15, and an $RMSE\%$ value of 14.03% when using calibration data from all growth stages; an R^2 value of 0.83, an $RMSE$ value of 0.14, and an $RMSE\%$ value of 14.29% when using calibration data from the Feekes 4 growth stage; and an R^2 value of 0.93, an $RMSE$ value of 0.14, and an $RMSE\%$ value of 12.17% when using the calibration data from the Feekes 7–8 growth stage. Meanwhile, the regression equations between $MTCI$ and the NNI resulted in an R^2 value of 0.79, an $RMSE$ value of 0.17, and an $RMSE\%$ value of 15.90% when using the calibration data from all growth stages; an R^2 value of 0.84, an $RMSE$ value of 0.10, and an $RMSE\%$ value of 10.20% when using the calibration data from the Feekes 4 growth stage; and an R^2 value of 0.92, an $RMSE$ value of 0.15, and an $RMSE\%$ value of 13.04% when using the calibration data from the Feekes 7–8 growth stage. The $MCARI$ and $TCARI$ values exhibited weak or no correlation with the NNI . The regression equation between the other indices and NNI had R^2 values between 0.52 and 0.75, $RMSE$ values between 0.19 and 0.24, and $RMSE\%$ values

between 17.77% and 22.45% when using the calibration data from all growth stages; R^2 values between 0.52 and 0.83, $RMSE$ values between 0.10 and 0.18, and $RMSE\%$ values between 10.20% and 18.37% when using the calibration data from the Feekes 4 growth stage; and R^2 values between 0.63 and 0.93, $RMSE$ values between 0.13 and 0.27, and $RMSE\%$ values between 11.30% and 23.48% when using the calibration data from the Feekes 7–8 growth stage. Therefore, the $REIP-LI$ and $MTCI$ were selected for estimating the NNI . The scatter plots between the $REIP-LI$ and NNI and between the $MTCI$ and NNI are shown in Figure 4a,b, respectively. The data from two growth stages generally formed two groups and slightly overlapped when plotted. Therefore, although good calibration results were obtained when using data from all growth stages, the phenology influenced the relationships between the NNI and the two spectral indices.

Table 6. Regression analysis results between all of the selected spectral indices and the NNI . Linear, logarithm, exponential, and power models were used for fitting. The results (R^2 , $RMSE$ and $RMSE\%$) of the best calibration models are shown.

Spectral Index	All Growth Stages ($n = 90$)		Feekes 4 Growth Stage ($n = 45$)		Feekes 7–8 Growth Stage ($n = 45$)	
	R^2 (Model)	$RMSE$ ($RMSE\%$)	R^2 (Model)	$RMSE$ ($RMSE\%$)	R^2 (Model)	$RMSE$ ($RMSE\%$)
$V_{i_{opt}}$	0.64 (Lin)	0.20 (18.71%)	0.76 (Exp)	0.13 (13.27%)	0.89 (Pow)	0.17 (14.78%)
$RVI I$	0.57 (Log)	0.22 (20.58%)	0.75 (Log)	0.12 (12.24%)	0.83 (Pow)	0.20 (17.39%)
$RVI II$	0.64 (Log)	0.20 (18.71%)	0.80 (Pow)	0.11 (11.22%)	0.89 (Pow)	0.17 (14.78%)
$MCARI/MTVI2$	0.75 (Pow)	0.20 (18.71%)	0.71 (Pow)	0.14 (14.29%)	0.80 (Pow)	0.23 (20.00%)
$REIP-LE$	0.71 (Pow)	0.19 (17.77%)	0.68 (Pow)	0.18 (18.37%)	0.78 (Exp)	0.21 (18.26%)
$DCNI$	0.68 (Pow)	0.22 (20.58%)	0.52 (Lin)	0.17 (17.35%)	0.73 (Pow)	0.26 (22.61%)
$MCARI$	0.17 (Log)	0.31 (29.00%)	0.35 (Pow)	0.20 (20.41%)	–	–
$TCARI$	–	–	0.21 (Pow)	0.22 (22.45%)	0.28 (Pow)	0.37 (32.17%)
$TCARI/OSAVI$	0.73 (Exp)	0.20 (18.71%)	0.69 (Exp)	0.14 (14.29%)	0.75 (Exp)	0.24 (20.87%)
$MTCI$	0.79 (Pow)	0.17 (15.90%)	0.84 (Pow)	0.10 (10.20%)	0.92 (Pow)	0.15 (13.04%)
$R-M$	0.67 (Log)	0.19 (17.77%)	0.83 (Pow)	0.10 (10.20%)	0.90 (Pow)	0.16 (13.91%)
CCI	0.60 (Lin)	0.22 (20.58%)	0.59 (Exp)	0.16 (16.33%)	0.63 (Pow)	0.27 (23.48%)
$REIP-LI$	0.80 (Lin)	0.15 (14.03%)	0.83 (Exp)	0.14 (14.29%)	0.93 (Pow)	0.14 (12.17%)
$NDVI$	0.52 (Lin)	0.24 (22.45%)	0.78 (Exp)	0.12 (12.24%)	0.84 (Exp)	0.19 (16.52%)
RVI	0.55 (Log)	0.23 (21.51%)	0.75 (Log)	0.12 (12.24%)	0.82 (Pow)	0.21 (18.26%)
EVI	0.69 (Lin)	0.19 (17.77%)	0.77 (Pow)	0.12 (12.24%)	0.93 (Pow)	0.13 (11.30%)
TVI	0.67 (Lin)	0.19 (17.77%)	0.74 (Pow)	0.13 (13.27%)	0.88 (Pow)	0.17 (14.78%)
$MSAVI$	0.67 (Lin)	0.19 (17.77%)	0.77 (Pow)	0.12 (12.24%)	0.93 (Pow)	0.13 (11.30%)
$OSAVI$	0.61 (Lin)	0.21 (19.64%)	0.78 (Pow)	0.12 (12.24%)	0.92 (Exp)	0.14 (12.17%)
$GNDVI$	0.63 (Lin)	0.21 (19.64%)	0.81 (Exp)	0.11 (11.22%)	0.89 (Exp)	0.17 (14.78%)
$MTVI2$	0.63 (Lin)	0.21 (19.64%)	0.76 (Pow)	0.12 (12.24%)	0.91 (Pow)	0.14 (12.17%)
$RTVI$	0.70 (Log)	0.19 (17.77%)	0.81 (Pow)	0.11 (11.22%)	0.93 (Pow)	0.13 (11.30%)

– indicates that significant ($p < 0.01$) correlations were not observed between the two variables; n indicates the sample number.

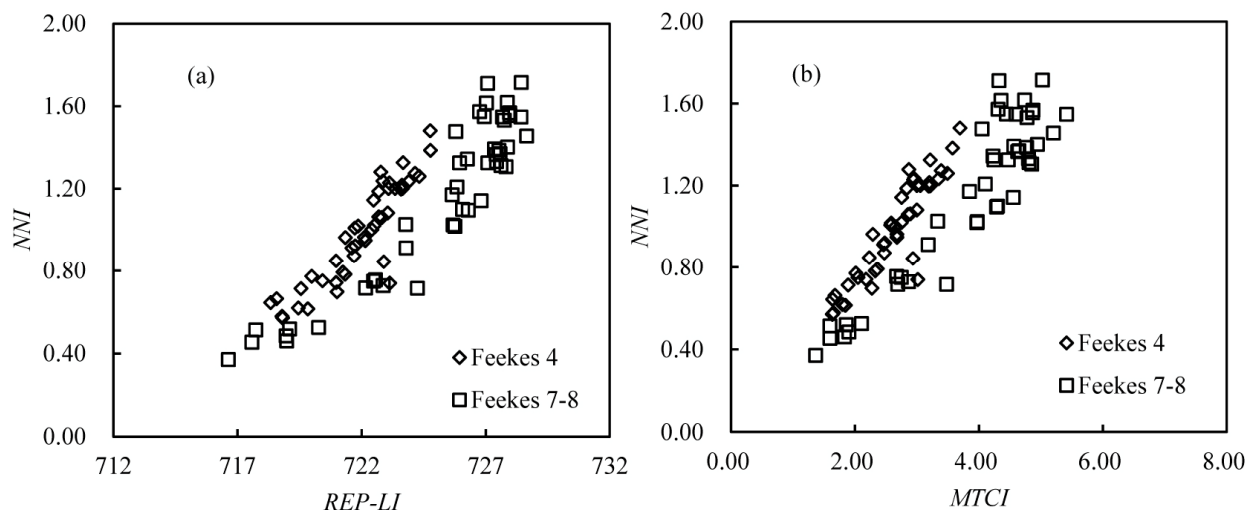


Figure 4. Scatterplots for (a) *REIP-LI* vs. *NNI* and (b) *MTCI* vs. *NNI*.

3.4. Validation of the *NNI* Estimation Models

Based on the above findings, for the mechanistic *NNI* estimation method, only the *NNI* assessment models using the *MCARI/MTVI2* and the *RTVI* were validated using the three validation datasets. Meanwhile, for the semi-empirical *NNI* estimation method, the *NNI* assessment models using the *REIP-LI* or *MTCI* were validated using three validation datasets. The validation results are listed in Table 7. For the *MCARI/MTVI2*- and *RTVI*-based *NNI* prediction models, the validation results showed that phenology had no influence on estimating the *NNI*. Regardless of whether the models were calibrated using data from all growth stages or data from a single growth stage, the models had similar performances when validated by the three validation datasets. The R^2 values varied from 0.85 to 0.89, the *RMSE* values varied from 0.11 to 0.13, and the *RMSE%* values varied from 10.18% to 12.04% when validated by data from all growth stages; the R^2 values varied from 0.93 to 0.94, the *RMSE* values varied from 0.05 to 0.06, and the *RMSE%* values varied from 5.10% to 6.12% when validated by data from the Feekes 4 growth stage; and the R^2 values varied from 0.82 to 0.86, the *RMSE* values varied from 0.15 to 0.17, and the *RMSE%* values varied from 12.71% to 14.41% when validated by data from the Feekes 7–8 growth stage. For the *MTCI*-based *NNI* prediction models and *REIP-LI*-based *NNI* prediction models, the influences of phenology can be observed from the validation results. For these models, the validation performance of the model was determined using the same types of samples in the calibration datasets. When the calibration dataset contained the proper amount of data collected at the same growth stage as the validation dataset, the validation results of the model were good. However, when the calibration dataset contained no data that were collected at the same growth stage as the validation dataset, the validation results of the model were worse. For the *MTCI* related *NNI* prediction models, the *RMSE* values varied from 0.13 to 0.25 and the *RMSE%* values varied from 12.03% to 23.15% when validated by data from all growth stages, the *RMSE* values varied from 0.05 to 0.23 and the *RMSE%* values varied from 5.10% to 23.47% when validated by data from the Feekes 4 growth stage, and the *RMSE* values varied from 0.13 to 0.35 and the *RMSE%* values varied from 11.02% to 29.66% when validated by data from the Feekes 7–8 growth stage. For the *REIP-LI*-based *NNI* prediction models, the *RMSE* values varied from 0.11 to 0.31 and the *RMSE%* values varied from 10.19% to 28.60% when validated by data from all growth stages, the *RMSE* values varied from 0.08 to 0.26 and the *RMSE%* values varied from 8.16% to

26.53% when validated by data from the Feekes 4 growth stage, and the *RMSE* values varied from 0.14 to 0.42 and the *RMSE%* values varied from 11.86% to 36.16% when validated by data from the Feekes 7–8 growth stage. Thus, the *NNI* estimation model when using the mechanistic method performed better when expanded to different growth stages than the *NNI* prediction model that was established using the semi-empirical method, at least between the Feekes 4 and Feekes 7–8 growth stages of wheat, which are critical stages for N topdressing.

Table 7. Validation results for the two *NNI* estimation method types.

Spectral Index Used in Model	Data Used for Model Establishment in Calibration Dataset	Validation by Data from All Growth Stages (<i>n</i> = 30)		Validation by Data from the Feekes 4 Growth Stage (<i>n</i> = 15)		Validation by Data from the Feekes 7–8 Growth Stage (<i>n</i> = 15)	
		<i>R</i> ²	<i>RMSE</i> (<i>RMSE%</i>)	<i>R</i> ²	<i>RMSE</i> (<i>RMSE%</i>)	<i>R</i> ²	<i>RMSE</i> (<i>RMSE%</i>)
<i>MCARI/MTVI2</i> and <i>RTVI</i>	All data (<i>n</i> = 90)	0.89	0.11 (10.18%)	0.94	0.06 (6.12%)	0.86	0.15 (12.71%)
<i>MCARI/MTVI2</i> and <i>RTVI</i>	Feekes 4 growth stage (<i>n</i> = 45)	0.88	0.12 (11.11%)	0.94	0.05 (5.10%)	0.86	0.16 (13.56%)
<i>MCARI/MTVI2</i> and <i>RTVI</i>	Feekes 7–8 growth stage (<i>n</i> = 45)	0.85	0.13 (12.04%)	0.93	0.06 (6.12%)	0.82	0.17 (14.41%)
<i>MTCI</i>	All data (<i>n</i> = 90)	0.86	0.13 (12.03%)	0.94	0.11 (11.22%)	0.90	0.14 (11.86%)
<i>MTCI</i>	Feekes 4 growth stage (<i>n</i> = 45)	0.85	0.25 (23.15%)	0.94	0.05 (5.10%)	0.90	0.35 (29.66%)
<i>MTCI</i>	Feekes 7–8 growth stage (<i>n</i> = 45)	0.85	0.19 (17.59%)	0.94	0.23 (23.47%)	0.90	0.13 (11.02%)
<i>REIP-LI</i>	All data (<i>n</i> = 90)	0.88	0.11 (10.19%)	0.91	0.08 (8.16%)	0.89	0.14 (11.86%)
<i>REIP-LI</i>	Feekes 4 growth stage (<i>n</i> = 45)	0.81	0.31 (28.60%)	0.94	0.10 (9.77%)	0.87	0.42 (36.16%)
<i>REIP-LI</i>	Feekes 7–8 growth stage (<i>n</i> = 45)	0.83	0.21 (19.44%)	0.94	0.26 (26.53%)	0.88	0.15 (12.71%)

4. Discussion

The *NNI* results estimated by remote sensing using existing methods are highly variable. Based on the *REIP-LI*, Mistele and Schmidhalter reported *R*² values of between 0.84 and 0.99 for winter wheat when predicting *NNI* values in southeast Germany [29]. Using a linear regression method, Liang and Liu reported an *R*² value of 0.91 for corn when estimating *NNI* values in northeastern China [30]. Chen *et al.* obtained an *R*² value of 0.81 for corn when estimating the *NNI* in the northwestern plains of Shandong province, China, based on the back-propagation of an Artificial Neural Networks model [55]. Thus, the results obtained in this study are within the range of previously published results.

For the practical use of *NNI* prediction approaches, the influences of external factors on these methods, such as sites, year, and phenology, must be known. This study conducted an innovation analysis and comparison of the effect of phenology on two types of existing *NNI* estimation methods,

the mechanistic method and the semi-empirical method. The study is very important for using remote sensing to predict the *NNI*. If the performance of an *NNI* prediction method is not influenced by phenology, it does not require collecting samples during each crop growth stage to design prediction models, which reduces the forecasting cost. In addition, different farmers do not always conduct farming activities at the same time. Thus, crops in different field are not always at the same growth stage during the growth season. In addition, the field N and other soil conditions vary significantly, which may result in phenology differences within a field. Because it is difficult to spatially determine the growth stage of a crop in detail [22] or to collect enough data to cover all prediction conditions for the phenology-influenced *NNI* prediction method to perform model calibration, methods that are insensitivity to phenology changes likely perform better when *NNI* prediction is conducted at a regional scale by using remote sensing sensors on planes or satellites. Based on the data in this study, the semi-empirical *NNI* prediction method is influenced more by phenology than the mechanistic method. This result can be explained as follows. (1) The existing index was designed to estimate chlorophyll, N, biomass, and the LAI to make it sensitive to objective factors while minimizing its sensitivity to other confounding factors [38]; (2) When using remote sensing to obtain the biomass and N concentration, which are used in the mechanistic model, studies of existing corresponding spectral indices have considered confounding factors such as phenology; (3) Because the *NNI* is calculated using biomass and N concentration, the detected spectral features for the *NNI* must be a combination of the spectral features of the LAI and chlorophyll (Table 3). However, no studies of spectral indices have been conducted that consider the above factors. Thus, the selected best *NNI* estimation indices in the semi-empirical method are sensitive to confounding factors such as phenology. In addition, these results suggest that the mechanistic method is better for predicting the *NNI*.

Remote sensing techniques have been used to conduct precise N management in the field [56–58]. Many variable-rate nitrogen application strategies have been proposed for N topdressing at critical crop growth stages based on remote detection of the N status of the crop [27]. Generally, the *NDVI* has been used as a crop N diagnosis tool in these studies. However, the *NDVI* is sensitive to many confounding factors, such as crop density and phenology. The *NNI* has been defined as a specific (varies only with nitrogen nutrition), sensitive (reacts rapidly to any change in plant N nutrition status), memorable (can give information about the history of the stand), and predictive (can infer future elements of crop behaviors) tool for crop N diagnosis [15]. Thus, smart N management can be improved by including the remotely sensed crop *NNI*. When the *NNI* is used for N management, existing variable-rate N application strategies can be adopted by making proper modifications. Additionally, for remote detection of the *NNI*, spectral data collected from crops with a tractor-mounted field spectrometer can be related to the *NNI* within a field [29]. By combining this method with a variable-rate computer controller mounted in a tractor, this type of data measurement can be used for precise N management “on-the-go”. In addition, airborne and satellite images can be used to produce spatially detailed *NNI* maps for large-scale applications.

5. Conclusions

Based on the use of a wide range of wheat data (three cultivars, different growth stages (Feekes 4 to Feekes 7–8)) and hyper-spectral data, the performances of two *NNI* estimation methods were evaluated. The mechanistic *NNI* prediction method performed well for estimating the *NNI* and was not

influenced by phenology. Meanwhile, the semi-empirical *NNI* prediction method performed well when a large enough database was collected for model calibration but was influenced by phenology, which limits its application in practice. Thus, the mechanistic *NNI* prediction method was recommended as a better method for estimating the *NNI*. By combining the *NNI* with a variable-N management strategy, the *NNI* can be used for precise N management in the field.

Acknowledgments

This research was supported by the National Natural Science Foundation of China (41301378) and the Science and Technology Basic Research Program of China (2014FY210150). In addition, we thank the six anonymous reviewers for their critical comments regarding the manuscript.

Conflicts of Interest

The author declares no conflict of interest.

References

1. Zhu, Y.; Yao, X.; Tian, Y.C.; Liu, X.J.; Cao, W.X. Analysis of common canopy vegetation indices for indicating leaf nitrogen accumulations in wheat and rice. *Int. J. Appl. Earth Obs.* **2008**, *10*, 1–10.
2. Mamo, M.; Malzer, G.L.; Mulla, D.J.; Huggins, D.R.; Stroock, J. Spatial and temporal variation in economically optimum nitrogen rate for corn. *Agron. J.* **2003**, *95*, 958–964.
3. Schröder, J.J.; Neeteson, J.J.; Oenema, O.; Struik, P.C. Does the crop or the soil indicate how to save nitrogen in maize production? Reviewing the state of the art. *Field Crop Res.* **2000**, *66*, 151–164.
4. Dambreville, C.; Morvan, T.; Germon, J.-C. N₂O emission in maize-crops fertilized with pig slurry, matured pig manure or ammonium nitrate in Brittany. *Agr. Ecosyst. Environ.* **2008**, *123*, 201–210.
5. Zhao, B.Z.; Zhang, J.B.; Flury, M.; Zhu, A.N.; Jiang, Q.A.; Bi, J.W. Ground water contamination with NO₃-N in a wheat-corn cropping system in the north China plain. *Pedosphere* **2007**, *17*, 721–731.
6. López-Bellido, L.; López-Bellido, R.J.; Redondo, R. Nitrogen efficiency in wheat under rainfed Mediterranean conditions as affected by split nitrogen application. *Field Crop Res.* **2005**, *94*, 86–97.
7. Justes, E.; Mary, B.; Meynard, J.M.; Machet, J.M.; Thelier-Huché, L. Determination of a critical nitrogen dilution curve for winter wheat crops. *Ann. Bot.* **1994**, *74*, 397–407.
8. Plénet, D.; Lemaire, G. Relationships between dynamics of nitrogen uptake and dry matter accumulation in maize crops. Determination of critical N concentration. *Plant Soil* **2000**, *216*, 65–82.
9. Ziadi, N.; Brassard, M.; Bélanger, G.; Cambouris, A.N.; Tremblay, N.; Nolin, M.C.; Claessens, A.; Parent, L.-É. Critical nitrogen curve and nitrogen nutrition index for corn in eastern Canada. *Agron. J.* **2008**, *100*, 271–276.
10. Ulrich, A. Physiological bases for assessing the nutritional requirements of plants. *Annu. Rev. Plant Physiol.* **1952**, *3*, 207–228.
11. Lemaire, G.; Gastal, F. N Uptake and distribution in plant canopies. In *Diagnosis on the Nitrogen Status in Crops*; Lemaire, G., Ed.; Springer-Verlag: Heidelberg, Germany, 1997; pp. 3–43.

12. Sheehy, J.E.; Dionara, M.J.A.; Mitchell, P.L.; Peng, S.; Cassman, K.G.; Lemaire, G.; Williams, R.L. Critical concentrations: Implications for high-yielding rice (*Oryza sativa* L.) cultivars in tropics. *Field Crop Res.* **1998**, *59*, 31–41.
13. Ziadi, N.; Bélanger, G.; Claessens, A.; Lefebvre, L.; Cambouris, A.N.; Tremblay, N.; Nolin, M.C.; Parent, L.-É. Determination of a critical nitrogen dilution curve for spring wheat. *Agron. J.* **2010**, *102*, 241–250.
14. Ziadi, N.; Bélanger, G.; Gastal, F.; Claessens, A.; Lemaire, G.; Tremblay, N. Leaf nitrogen concentration as an indicator of corn nitrogen status. *Agron. J.* **2009**, *101*, 947–957.
15. Lemaire, G.; Marie-Hélène, J.; François, G. Diagnosis tool for plant and crop N status in vegetative stage theory and practices for crop N management. *Eur. J. Agron.* **2008**, *28*, 614–624.
16. Clevers, J.G.P.W.; Gitelson, A.A. Remote estimation of crop and grass chlorophyll and nitrogen content using red-edge bands on Sentinel-2 and -3. *Int. J. Appl. Earth Obs.* **2013**, *23*, 344–351.
17. Haboudane, D.; Miller, J.R.; Pattey, E.; Zarco-Tejada, P.J.; Strachan, I.B. Hyperspectral vegetation indices and novel algorithms for predicting green LAI of crop canopies: Modeling and validation in the context of precision agriculture. *Remote Sens. Environ.* **2004**, *90*, 337–352.
18. Thomas, V.; Treitz, P.; Mccaughey, J.H.; Noland, T.; Rich, L. Canopy chlorophyll concentration estimation using hyperspectral and lidar data for a boreal mixedwood forest in northern Ontario, Canada. *Int. J. Remote Sens.* **2008**, *29*, 1029–1052.
19. Curran, P.J. Remote sensing of foliar chemistry. *Remote Sens. Environ.* **1989**, *30*, 271–278.
20. Fourty, Th.; Baret, F.; Jacquemoud, S.; Schmuck, G.; Verdebout, J. Leaf optical properties with explicit description of its biochemical composition: Direct and inverse problems. *Remote Sens. Environ.* **1996**, *56*, 104–117.
21. Kokaly, R.F.; Clark, R.N. Spectroscopic determination of leaf biochemistry using band-depth analysis of absorption features and stepwise multiple linear regression. *Remote Sens. Environ.* **1999**, *67*, 267–287.
22. Chen, P.; Haboudane, D.; Tremblay, N.; Wang, J.; Vigneault, P.; Li, B. New spectral indicator assessing the efficiency of crop nitrogen treatment in corn and wheat. *Remote Sens. Environ.* **2010**, *114*, 1987–1997.
23. Boochs, F.; Kupfer, G.; Dockter, K.; Kühbauch, W. Shape of the red-edge as vitality indicator for plants. *Int. J. Remote Sens.* **1990**, *11*, 1741–1753.
24. Madakadze, I.C.; Madakadze, R.M. Field evaluation of the chlorophyll meter to predict yield and nitrogen concentration of switchgrass. *J. Plant Nutr.* **1999**, *22*, 1001–1010.
25. Cartelat, A.; Cerovic, Z.G.; Goulas, Y.; Meyer, S.; Lelarge, C.; Prioul, J.L.; Barbottin, A.; Jeuffroy, M.H.; Gate, P.; Agati, G.; *et al.* Optically assessed contents of leaf polyphenolics and chlorophyll as indicators of nitrogen deficiency in wheat (*Triticum aestivum* L.). *Field Crop Res.* **2005**, *91*, 35–49.
26. Hansen, P.M.; Schjoerring, J.K. Reflectance measurement of canopy biomass and nitrogen status in wheat crops using normalized difference vegetation indices and partial least squares regression. *Remote Sens. Environ.* **2003**, *86*, 542–553.
27. Cilia, C.; Panigada, C.; Rossini, M.; Meroni, M.; Busetto, L.; Amaducci, S.; Boschetti, M.; Picchi, V.; Colombo, R. Nitrogen status assessment for variable rate fertilization in maize through hyperspectral imagery. *Remote Sens.* **2014**, *6*, 6549–6565.

28. Chen, P. Research on New Hyperspectral Indices for Plant Nitrogen Concentration and Biomass Estimation and Their Applications. Ph.D. Dissertation, China Agricultural University, Beijing, China, 2009. (In Chinese with English Abstract)
29. Mistele, B.; Schmidhalter, U. Estimating the nitrogen nutrition index using spectral canopy reflectance measurements. *Eur. J. Agron.* **2008**, *29*, 184–190.
30. Liang, H.; Liu, X. Model for calculating corn nitrogen nutrition index using hyper-spectral data. *Trans. CSAE* **2010**, *26*, 250–255. (In Chinese)
31. Miller, T.D. Growth stages of wheat: Identification and understanding improve crop management. *Better Crops.* **1992**, *76*, 12–17.
32. Chen, P.; Zhu, Y. A new method for winter wheat critical nitrogen curve determination. *Agron. J.* **2013**, *105*, 1839–1836.
33. Lemaire, G.; Meynard, J.M. Use of the Nitrogen Nutrition Index for analysis of agronomical data. In *Diagnosis on the Nitrogen Status in Crops*; Lemaire, G., Ed.; Springer-Verlag: Heidelberg, Germany, 1997; pp. 45–55.
34. Reyniers, M.; Walvoort, D.J.J.; de Baardemaaker, J. A linear model to predict with a multi-spectral radiometer the amount of nitrogen in winter wheat. *Int. J. Remote Sens.* **2006**, *27*, 4159–4179.
35. Xue, L.H.; Cao, W.X.; Luo, W.H.; Dai, T.B.; Zhu, Y. Monitoring leaf nitrogen status in rice with canopy spectral reflectance. *Agron. J.* **2004**, *96*, 135–142.
36. Eitel, J.U.H.; Long, D.S.; Gessler, P.E.; Smith, A.M.S. Using *in situ* measurements to evaluate the new RapidEye™ satellite series for prediction of wheat nitrogen status. *Int. J. Remote Sens.* **2007**, *28*, 4183–4190.
37. Cho, M.A.; Skidmore, A.K. A new technique for extracting the red edge position from hyperspectral data: The linear extrapolation method. *Remote Sens. Environ.* **2006**, *101*, 181–193.
38. Daughtry, C.S.T.; Walthall, C.L.; Kim, M.S.; de Colstoun, E.B.; McMurtrey, J.E., III. Estimating corn leaf chlorophyll concentration from leaf and canopy reflectance. *Remote Sens. Environ.* **2000**, *74*, 229–239.
39. Haboudane, D.; Miller, J.R.; Tremblay, N.; Zarco-Tejada, P.J.; Dextraze, L. Integrated narrow-band vegetation indices for prediction of crop chlorophyll content for application to precision agriculture. *Remote Sens. Environ.* **2002**, *81*, 416–426.
40. Haboudane, D.; Tremblay, N.; Miller, J.R.; Vigneault, P. Remote estimation of crop chlorophyll content using spectral indices derived from hyperspectral data. *IEEE Trans. Geosci. Remote Sens.* **2008**, *46*, 423–437.
41. Dash, J.; Curran, P.J. The MERIS terrestrial chlorophyll index. *Int. J. Remote Sens.* **2004**, *25*, 5003–5013.
42. Gitelson, A.A.; Viña, A.; Ciganda, V.; Rundquist, D.C. Remote estimation of canopy chlorophyll content in crops. *Geophys. Res. Lett.* **2005**, *32*, L08403.
43. Sims, D.A.; Luo, H.Y.; Hastings, S.; Oechel, W.C.; Rahman, A.F.; Gamon, J.A. Parallel adjustments in vegetation greenness and ecosystem CO₂ exchange in response to drought in a southern California chaparral ecosystem. *Remote Sens. Environ.* **2006**, *103*, 289–303.
44. Guyot, G.; Baret, F.; Major, D.J. High spectral resolution: Determination of spectral shifts between the red and the near infrared. *ISPRS J. Photogramm.* **1988**, *11*, 740–760.

45. Rouse, J.W.; Haas, R.H.; Schell, J.A.; Deering, D.W.; Harlan, J.C. *Monitoring the Vernal Advancement of Retrogradation (Green Wave Effect) of Natural Vegetation*; Type III, Final Report; NASA/GSFC: Greenbelt, MD, USA, 1974; p. 371.
46. Pearson, R.L.; Miller, L.D. *Remote Mapping of Standing Crop Biomass for Estimation of the Productivity of the Short-Grass Prairie, Pawnee National Grasslands, Colorado*; ERIM: Ann Arbor, MI, USA, 1972.
47. Huete, A.; Justice, C.; Liu, H. Development of vegetation and soil indices for MODIS. *Remote Sens. Environ.* **1994**, *49*, 224–234.
48. Broge, N.H.; Leblanc, E. Comparing prediction power and stability of broadband and hyperspectral vegetation indices for estimation of green leaf area index and canopy chlorophyll density. *Remote Sens. Environ.* **2001**, *76*, 156–172.
49. Qi, J.; Chehbouni, A.; Huete, A.R.; Kerr, Y.H.; Sorooshian, S. A modified soil adjusted vegetation index. *Remote Sens. Environ.* **1994**, *48*, 119–126.
50. Rondeaux, G.; Steven, M.; Baret, F. Optimization of soil-adjusted vegetation indices. *Remote Sens. Environ.* **1996**, *55*, 95–107.
51. Gitelson, A.A.; Kaufman, Y.; Merzlyak, M. Use of a green channel in remote sensing of global vegetation from EOS-MODIS. *Remote Sens. Environ.* **1996**, *58*, 289–298.
52. Chen, P.; Tremblay, N.; Wang, J.; Vigneault, P.; Huang, W.; Li, B. New index for crop canopy fresh biomass estimation. *Spectrosc. Spect. Anal.* **2010**, *30*, 512–517. (In Chinese)
53. Lemaire, G.; van Oosterom, E.; Sheehy, J.; Jeuffroy, M.H.; Massignam, A.; Rossato, L. Is crop N demand more closely related to dry matter accumulation or leaf area expansion during vegetative growth? *Field Crop Res.* **2007**, *100*, 91–106.
54. Gitelson, A.A. Wide dynamic range vegetation index for remote quantification of biophysical characteristics of vegetation. *J. Plant Physiol.* **2004**, *161*, 165–173.
55. Chen, P.; Wang, J.; Huang, W.; Tremblay, N.; Ou, Y.; Zhang, Q. Critical nitrogen curve and remote detection of nitrogen nutrition index for corn in the northwestern plain of Shandong province, China. *IEEE J.-STARS* **2013**, *6*, 682–689.
56. Lukina, E.V.; Freeman, K.W.; Wynn, K.J.; Thomason, W.E.; Mullen, R.W.; Klatt, A.R.; Johnson, G.V.; Elliott, R.L.; Stone, M.L.; Solie, J.B.; *et al.* Nitrogen fertilization optimization algorithm based on in-season estimates of yield and plant nitrogen uptake. *J. Plant Nutr.* **2001**, *24*, 885–898.
57. Raun, W.R.; Solie, J.B.; Stone, M.L.; Martin, K.L.; Freeman, K.W.; Mullen, R.W.; Zhang, H.; Schepers, J.S.; Johnson, G.V. Optical sensor based algorithm for crop nitrogen fertilization. *Commun. Soil Sci. Plant Anal.* **2005**, *36*, 2759–2781.
58. Zhao, C.; Chen, P.; Huang, W.; Wang, J.; Wang, Z.; Jiang, A. Effects of two kinds of variable-rate nitrogen application strategies on the production of winter wheat (*Triticum aestivum*). *N. Z. J. Crop Hort.* **2009**, *37*, 149–155.